Nanoscale Advances

ROYAL SOCIETY OF CHEMISTRY

PAPER

View Article Online
View Journal | View Issue

Cite this: *Nanoscale Adv.*, 2026, **8**, 1949

Crosslinked, organic solvent resistant ethylcellulose micro and nanocapsules for heterogeneous catalysis applications

Erika Ghiglietti, Sara Mecca, Alice Fappani, Annapia Fratepietro, Sara Mattiello * and Luca Beverina *

Received 27th January 2026
Accepted 31st January 2026

DOI: 10.1039/d6na00071a

rsc.li/nanoscale-advances

Encapsulation, a widely employed technology with applications across diverse industrial fields, involves the incorporation of active compounds within a protective coating layer. Although numerous synthetic strategies are described in the literature, sustainability remains a significant concern. Here, we report a sustainable, mini-emulsion solvent evaporation (MESE)-based protocol for producing bio-based and crosslinked micro- and nanocapsules using ethylcellulose (EC) as the biopolymeric shell. Remarkably, crosslinking is performed directly in aqueous dispersion, minimizing the use of organic solvents. The robustness of the methodology is demonstrated using several hydrophobic payloads, and the protocol is specifically optimized for palladium(II) catalysts. The resulting heterogeneous, supported catalysts efficiently promote cross-coupling reactions in water at remarkably low catalyst loadings.

Introduction

Over the past decades, interest in sustainable and scalable methods for producing micro- and nanocapsules has expanded rapidly.[1–3] Encapsulation is widely applied in numerous industrial sectors, including personal care, cosmetics, agrochemicals, textiles, medicine, and food packaging.[4–6] The key advantages of encapsulation lie in protecting the cargo from external degradation and enabling controlled release kinetics.[7–11] Furthermore, the functionalization of encapsulating materials allows for the creation of stimuli-responsive systems, whose release profiles can be tuned by environmental changes such as pH, temperature, or light exposure. Nanoencapsulation, in particular, holds great promise for targeted drug delivery due to efficient cellular uptake and site-specific release.[1,2,12]

A variety of chemical, physicochemical, and mechanical methods have been employed for capsule fabrication, including interfacial and *in situ* polymerization, coacervation–phase separation, and spray-drying.[10,13–17] While many of these methods yield microcapsules, producing nanocapsules remains more challenging. Among laboratory-scale methods, mini emulsion solvent evaporation (MESE) offers a practical and efficient route that requires no specialized equipment.[17–20] This technique involves emulsifying a water-immiscible volatile solvent containing the polymer and payload within an aqueous surfactant phase, followed by solvent evaporation under stirring. The resulting capsules can be recovered by filtration or centrifugation, depending on size. To minimize leakage of encapsulated material, an additional crosslinking step is typically required.[21,22] Among encapsulating materials, ethylcellulose (EC) is particularly attractive due to its non-toxicity, biocompatibility, thermal and chemical stability, and derivation from renewable biomass.[23–25] Its hydrophobicity and solubility in benign solvents such as ethyl acetate make it an ideal choice for hydrophobic cargos.[26–29]

However, traditional microencapsulation approaches become inefficient when targeting capsules in the nanometric range, primarily due to low recovery yields. Consequently, many applications rely directly on aqueous dispersions without isolation or purification.[19] Another significant limitation is the reliance on toxic crosslinkers, such as formaldehyde.[22,26,30–32]

Herein, we present a general and sustainable method for the preparation and high-yield recovery of crosslinked ethylcellulose micro- and nanocapsules. The strategy employs a non-toxic crosslinker, 1,2,3,4-butanetetracarboxylic acid (BTCA), known for crosslinking cellulose in bulk and film,[30,33–36] but has never been applied as an *in situ* crosslinker for nanocapsule systems. We demonstrate that capsule size, crosslinking degree, and loading efficiency can be readily tuned. Moreover, the pH-dependent carboxylic functionalities introduced *via* BTCA promote efficient crosslinking and facilitate easy capsule recovery regardless of size.

To showcase the versatility of the method, we further demonstrate that incorporation of a palladium catalyst into the EC nanocapsules yields efficient heterogeneous nanoreactors capable of catalyzing Sonogashira cross-coupling reactions in water under micellar catalysis conditions.

Department of Materials Science, University of Milano-Bicocca, via Cozzi 55, 20126 Milano, Italy. E-mail: sara.mattiello@unimib.it; luca.beverina@unimib.it

Results and discussion

Preparation of micro- (Mcs) and nanocapsules (Ncs) by the MESE technique

Our approach for synthesizing crosslinked ethylcellulose (EC) micro- and nanocapsules is based on the MESE technique. The key advancement compared to previous methods lies in the *in situ* crosslinking using BTCA, which produces stable nanocapsules while significantly improving recovery yield (see *infra*).

Fig. 1 illustrates the general workflow for preparing both spheres and loaded capsules.

The optimized methodology comprises three main steps: (1) emulsification and homogenization, followed by probe sonication for nanocapsules; (2) *in situ* crosslinking; (3) hardening with sodium tetraborate decahydrate (borax).

For the first step, we initially started studying the process using EC only as the shell material, however we later found that the same procedure can be applied to cellulose pre-functionalized with epoxides (see *infra*). Vanillin was chosen as a model hydrophobic cargo, as its release profile could be conveniently monitored. Both dichloromethane and ethyl acetate were evaluated as solvents for the oil phase; the latter was ultimately selected due to its lower toxicity and cost. Polyvinyl alcohol (PVA) was employed as the surfactant in the aqueous phase, as it offers efficient emulsification and excellent film-forming capability.

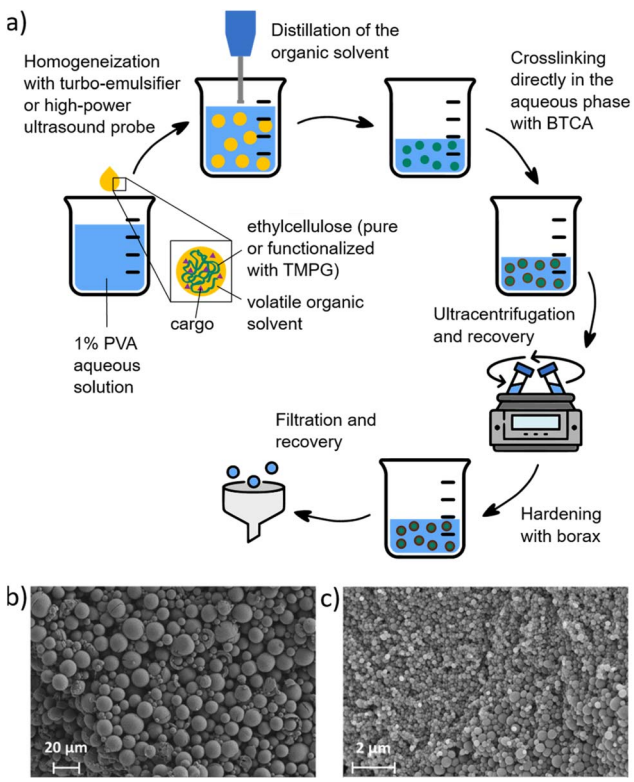

Fig. 1 (a) Synthetic scheme for the preparation of both micro- and nano-capsules *via* the modified MESE method, and SEM images of unloaded (b) microcapsules ($d \approx 10$–20 µm) and (c) nanocapsules ($d \approx 60$–80 nm) of EC.

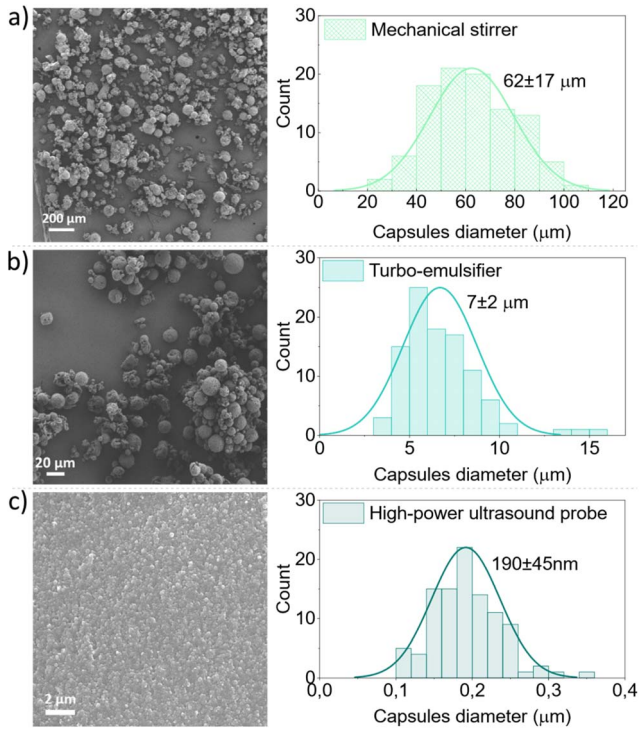

Fig. 2 SEM images of EC capsules prepared using different mixing methods during the emulsification step. (a) Mechanical stirring (500 rpm); (b) ultra-turrax (14 000 rpm); (c) high-power ultrasound probe (cycle 50%, amplitude 50%, 10 minutes) and distributions of the diameters of the particles, fitted with a gaussian curve.

We systematically investigated how process parameters—such as the presence/absence of a cargo, EC concentration in the oil phase, and stirring speed—affect the resulting capsule morphology (details in the SI, Sections 3 and 8). The emulsification method emerged as the dominant factor influencing capsule size. In fact, switching from standard magnetic or mechanical stirring to high-power ultrasonication enabled a controlled transition from micro- to nanoscale particles (Fig. 2 and Table 1, entries 1–3).

Probe sonication efficiently refines emulsion droplet size, preventing aggregation and ensuring uniform nanoscale dispersion.[37,38] After emulsification, capsule formation was achieved by solvent removal. Both evaporation at atmospheric pressure and under reduced pressure were tested, leading to the same results. We ultimately decided to resort to distillation under reduced pressure as it's faster and it allows for solvent recovery.

BTCA induced crosslinking of Mcs and Ncs

We next optimized the BTCA-mediated crosslinking step. Mechanistically, BTCA crosslinking proceeds *via* two steps: formation of a cyclic anhydride intermediate, followed by esterification between the anhydride and cellulose hydroxyl groups. This mechanism has been well documented for cellulose-based materials[36,37] and it is here adapted for the nanoscale. Traditional solid-phase methods (immersion in

Table 1 Effect of emulsifying method on the final size of capsules. All samples are prepared using 5 wt% of EC in AcOEt and vanillin as a cargo

Entry	Mixing method (rpm)	Crosslinker	Avg. dimensions[a]	Mass recovery
1	Mechanical stirrer (500)	—	62 ± 17 μm	[b]50%
2	Turbo-emulsifier	—	7 ± 2 μm	45 ± 4%
3	Ultrasound probe	—	190 ± 45 nm	33 ± 3%
4	Ultrasound probe	BTCA	270 ± 96 nm	75 ± 6%

[a] Average dimensions of capsules are calculated from SEM images over a sample of 100 objects. Values are reported as mean ± standard deviation. [b] Single experiment.

BTCA and catalyst solutions followed by oven curing at 120–150 °C) led to undesirable particle sintering, forming solid aggregates rather than discrete capsules (see also the SI, Section 6.1). To overcome this, we developed a wet crosslinking protocol, heating the as-prepared capsule suspension at 90 °C for six hours in an aqueous BTCA/NaH_2PO_4 solution. Electrostatic repulsion among dispersed particles prevents coalescence, enabling uniform and individual capsule crosslinking. This step also proved essential for optimizing recovery: while microcapsules could be recovered easily by filtration or centrifugation, non-crosslinked nanocapsules yielded less than 30% after ultracentrifugation. By contrast, crosslinking directly in aqueous dispersion raised the recovery to over 70% of theoretical yield (Table 1, entry 3–4).

Crosslinked capsules were characterized by NMR, FTIR, SEM, DSC, TGA, and DLS (see the SI, Section 6, 7.1 and 9). Fig. 3a and b shows the SEM images of both non-crosslinked and crosslinked nanocapsules. An increase in the average dimensions upon crosslinking is observed (Table 1, entry 3–4), which is attributed to the formation of the BTCA ester polymeric shell, possibly in combination with residual PVA incorporation. The occurrence of the crosslinking is also supported by FT-IR analysis. Fig. 3c reports a comparison between FT-IR spectra of pristine ethylcellulose, vanillin, non-crosslinked and BTCA-crosslinked Ncs.

The incorporation of vanillin is demonstrated by the presence of the characteristic peaks of the cargo in the spectrum (region between 1300 and 1600 cm^{-1}). The vanillin peaks in crosslinked capsules are weaker, hinting at preferential localization in the core. The presence of a new peak at 1739 cm^{-1} in the spectrum of the crosslinked Ncs (stretching of C=O) is attributed to esterification of BTCA with EC and residual PVA, possibly to form an outer shell.[39] The reduction of intensity of the O–H stretching (around 3500 cm^{-1}) also hints at the occurrence of the esterification reaction.

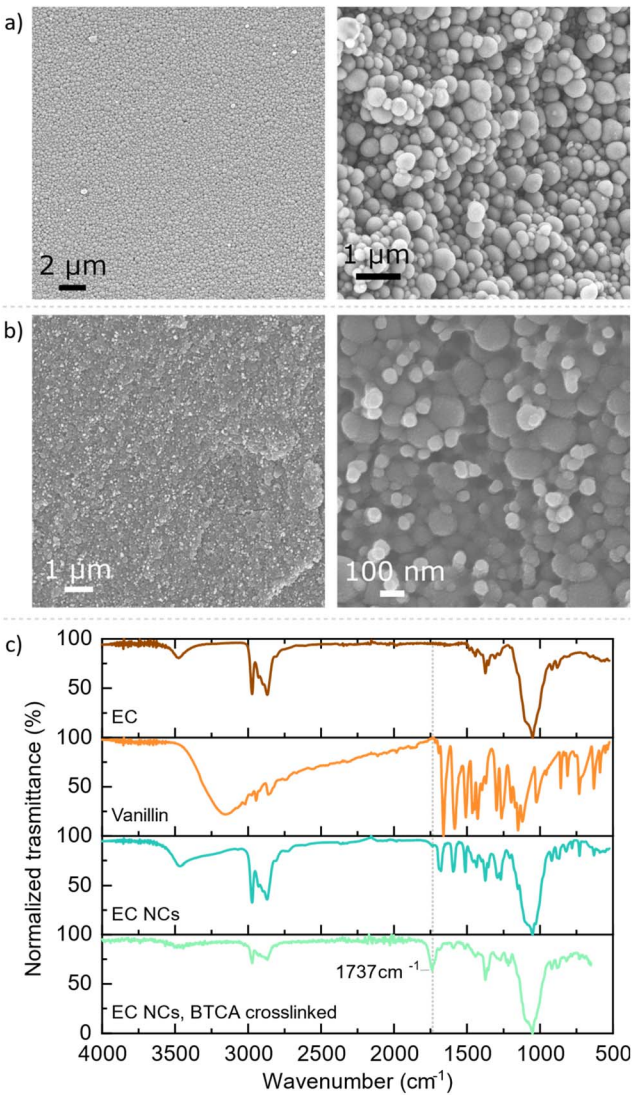

Fig. 3 SEM images of loaded nanocapsules prepared according to the general procedure. (a) Non-crosslinked; (b) crosslinked with BTCA. (c) FT-IR spectra comparisons of EC, vanillin, non-crosslinked nanocapsules and capsules crosslinked with BTCA.

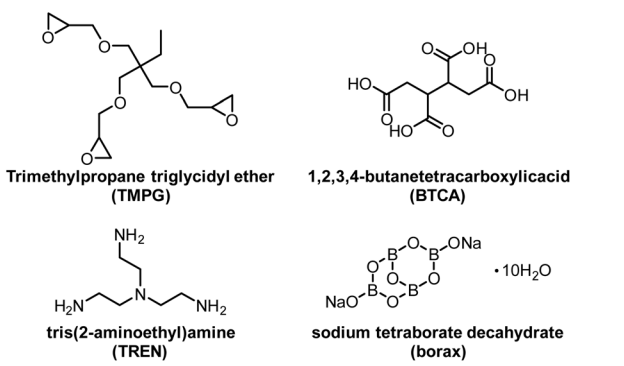

Scheme 1 Chemical structure of the crosslinking agents employed for the hardening of EC capsules.

We also verified that, at the end of the crosslinking procedure, the excess unreacted BTCA can be easily recovered by selective precipitation, thus improving on the overall sustainability of the approach (see the SI, Section 10 for details).

Synergistic BTCA, epoxy and primary amine crosslinking

To explore synergistic effects, we combined BTCA with additional crosslinking and hardening agents: the epoxide trimethylpropane triglycidyl ether (TMPG), the multifunctional amine tris(2-aminoethyl)amine (TREN), and sodium tetraborate (borax) (Scheme 1).

Differently from all other crosslinkers, TMPG was added directly in the initial EC organic solution before capsule preparation, with the idea of introducing epoxide groups capable of additional crosslinking during BTCA curing. The EC chemical modification over time was thoroughly characterized by ^{1}H NMR and viscosity analysis (Section 4 of the SI). Using TMPG-functionalized EC in MESE encapsulation, followed by BTCA crosslinking, we obtained smaller capsules with a denser polymeric network. Table 2 shows a comparison between BTCA-crosslinked samples, TMPG-crosslinked ones, and their combination.

Table 2 Effect of crosslinking on the size of Ncs. All samples are prepared according to the general procedure using 5 wt% of EC in AcOEt (see also Table S1, Section S5 of the SI). A high-power ultrasound probe is used as the homogenizer

Entry	Cargo	Crosslinker	Avg. dimensions[a]
1	Vanillin	—	190 ± 45 nm
2	Vanillin	BTCA	270 ± 96 nm
3	Vanillin	TMPG	167 ± 35 nm
4	Vanillin	TMPG-BTCA	217 ± 60 nm
5	—	TMPG-BTCA	96 ± 40 nm
6	Vanillin	TMPG-TREN	170 ± 40 nm
7	—	TMPG-BTCA + borax	117 ± 40 nm

[a] Average dimensions of capsules are measured from SEM images (SI, Section 7.2) over a sample of 100 objects. Values are reported as mean ± standard deviation.

FTIR spectra (SI, Section S7.2, Fig. S12) of Ncs produced using TMPG functionalized EC do not differ substantially from those of EC only. On the other side, Ncs treated with BTCA display the same previously observed ester stretching at 1737 cm^{-1}, supporting the occurrence of crosslinking. Thermal analyses (Fig. 4) revealed that TMPG pre-treated capsules crosslinked with BTCA exhibit superior thermal stability with respect to capsules treated with BTCA or TMPG separately. In fact, DSC traces show that the capsule softening temperature for the TMPG + BTCA crosslinked material is around 225 °C, higher than that of both BTCA (187 °C) and TMPG (209 °C) singularly treated (Fig. 4a). Moreover, we observed a fourfold lower melting grade for Ncs treated with both TMPG and BTCA at 190 °C, indicative of a synergistic strengthening effect (Fig. 4b). This effect directly translates into an improved thermal stability of the material.

In fact, vanillin loaded Ncs prepared with TMPG functionalized EC treated at 120 °C for two hours (*i.e.*, above the melting point of vanillin) melt due to dissolution of the polymeric shell into the molten cargo. On the other side, capsules treated with both TMPG and BTCA remain solid when subject to the same thermal treatment (Fig. 4c).

To understand if crosslinking was suitable to improve the capsules' solvent resistance, we recorded DLS of unloaded Ncs in different solvents before and after treatment with BTCA. While TMPG functionalized EC is soluble in all the tested organic solvents, BTCA crosslinked Ncs remain intact in protic polar solvents such as methanol and ethanol (SI, Fig. S21).

Finally, we also tested the addition of TREN instead of BTCA in the crosslinking step of EC-TMPG, finding that it provides

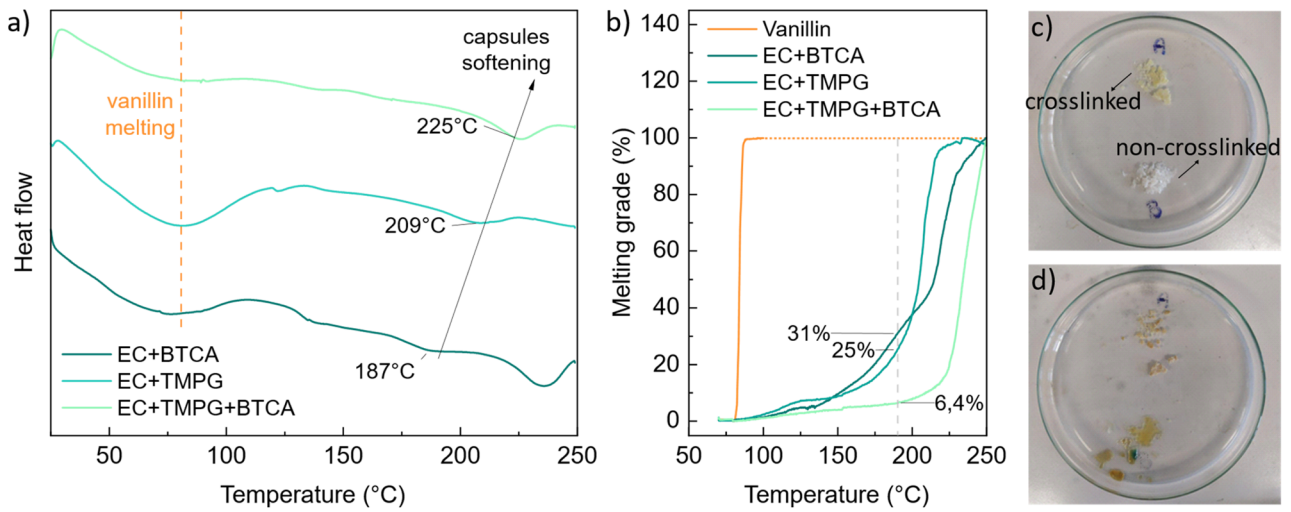

Fig. 4 Thermal characterization of crosslinked nanocapsules. (a) DSC measurements of vanillin loaded Ncs crosslinked with either BTCA, TMPG or both. Vanillin melting is always observed at the same temperature (around 82 °C), while capsule softening temperature varies. (b) Melting grade of pure vanillin, and vanillin loaded Ncs crosslinked with either BTCA, TMPG or both. Digital images of BTCA crosslinked (A) and non-crosslinked (B) Ncs loaded with vanillin, before (c) and after (d) a thermal treatment of 2 hours at 120 °C.

further crosslinking at lower curing temperatures – an advantage when encapsulating thermally sensitive cargos (details in Section 7.3 of the SI).

Hardening with boric acid

BTCA crosslinked capsules can be further hardened by the action of sodium tetraborate decahydrate ($Na_2B_4O_7 \cdot 10H_2O$, also known as borax), a crosslinking agent already used for biomedical applications.[40] Upon dissolution in water, borax is fully converted into boric acid ($B(OH)_3$) and monoborate anions ($B(OH)_4^-$), which complex with hydroxyl functionalities of EC, creating a robust polymer network around the cargo through hydrogen and covalent bonds. This hardening step is performed after redispersion of BTCA-crosslinked nanocapsules in an aqueous borax solution and it involves a wet-thermal treatment at 90 °C for 3 h. After cooling, the precipitate can be easily separated by filtration on a paper funnel, yielding a quantitative mass recovery of crosslinked nanocapsules.

After borax crosslinking, the surface of the resulting objects remained smooth and no signs of aggregation are observed through SEM analysis of samples (SI, Section 7.4, Fig. S16). Furthermore, the dispersibility of capsules in water after their isolation is investigated, showing an enhanced hydrophilicity of the materials when going from pristine ethylcellulose to capsules crosslinked with both BTCA and borax, confirming a modification of the polymer shell (Fig. 5a). The higher dispersibility in water of borax hardened Ncs is also observed by DLS (Fig. 5b). In fact, the average diameter observed for BTCA only crosslinked Ncs is 295 nm, way higher than the average of 96 nm measured by SEM. This is due to the aggregation of the particles in the aqueous medium. The hydrodynamic diameter observed for borax hardened particles, on the other side, is 190 nm. They appear smaller than BTCA only crosslinked Ncs, even though they are bigger according to SEM (117 nm on average). This is due to the better dispersibility of such capsules, possibly due to the presence of superficial negatively charged sites.

Finally, DLS of hardened Ncs was also recorded in organic solvents. Besides polar protic solvents, the capsules proved to be resistant also in several aprotic polar ones, such as ethyl acetate, acetonitrile and tetrahydrofuran (SI, Fig. S21).

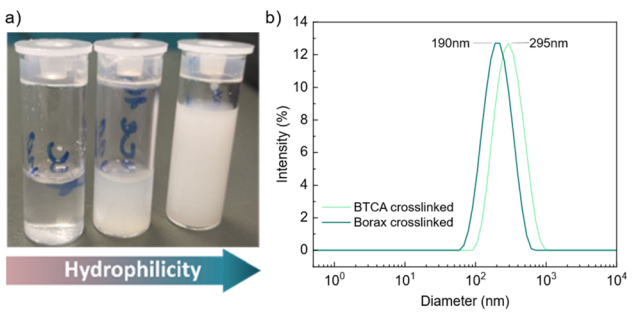

Fig. 5 (a) Picture of pristine EC, Ncs crosslinked with BTCA only, and Ncs crosslinked with BTCA and borax in deionized water, respectively. (b) DLS of Ncs crosslinked with BTCA only, and BTCA and borax.

Greenness methodology evaluation

With the aim of highlighting the greenness and efficacy of our crosslinking approach compared to literature-derived methods, herein we report both the calculation of process mass intensity (PMI) and the recovery efficiency for each crosslinking method we tested (Fig. 6 and SI, Section 12). In terms of efficiency, the syntheses of both non-crosslinked nanocapsules and those crosslinked using literature methods result in low particle recovery yields (33% and 16%, respectively). In contrast, our proposed crosslinking approaches lead to a significant increase in the mass recovery efficiency due to the reduction of isolation steps, as the BTCA crosslinking is performed *in situ*, without prior capsule isolation. Since the PMI is defined as the ratio of the mass of waste per mass of product, it is evident that recovery efficiency has a substantial impact on this green metric. In this context, the lack of crosslinking (190) and crosslinking procedure according to the literature (637) are negatively affected by the loss of material due to the softness of the polymer outer shell and the presence of an additional isolation step required prior to the crosslinking, respectively. In comparison, the proposed methodologies provide a far better result with PMI of 83.2 and 137 for the overall process, thanks to the optimization of the crosslinking procedure.

Our analysis is performed on the laboratory scale, therefore we did not consider energy consumption metrics, which are fundamental to understanding the effective sustainability of a process. We want to emphasize that this analysis is only comparative with the BTCA crosslinking procedure made in bulk. Our aim was to demonstrate that our *in situ* crosslinking methodology is simple, time-efficient and scalable, and it also appears to be more sustainable compared to other approaches thanks to the higher recovery achievable.

Evaluation as heterogenized nano-catalysts for Sonogashira coupling reactions

The robustness of the developed nanocapsules prompted us to test their possible use as supports to obtain heterogeneous

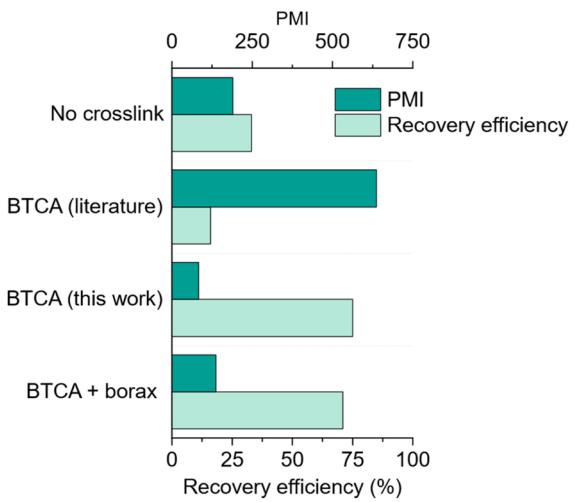

Fig. 6 Comparison of sustainability and efficiency of our approach compared to the literature derived one: estimation of PMI and recovery efficiency for every procedure.

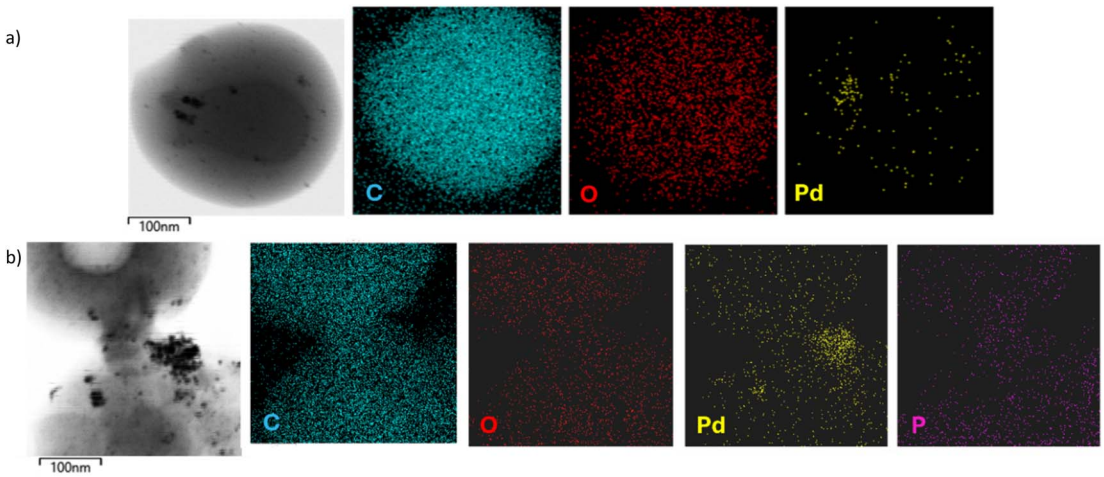

Fig. 7 High resolution transmission electron microscopy (HR-TEM) images of EC-nanocapsules loaded with (a) palladium acetate or (b) both palladium acetate and XPhos ligand and the corresponding mapping images: C, O, Pd and P are detected.

palladium catalysts suitable to promote cross-coupling reactions under micellar catalysis conditions. In particular, we decided to use borax-crosslinked capsules due to their capability to withstand organic solvents, which are typically needed for purification procedures.

We considered the encapsulation of several palladium(II) catalysts and/or phosphine ligands, which are well-documented in the literature for their efficacy in promoting cross-coupling reactions.[41,42] Literature approaches within this field have used cellulose polymers only as scaffolds for Pd nanoparticles, whilst the use of an encapsulation approach is original.[2,12,29] Our strategy enables the assembling of EC-based "nanoreactors" for catalysis applications, where the catalytic species should be ideally localized into the apolar pockets of the encapsulating material. This arrangement should not provide for rate acceleration, it rather offers the advantage of protecting the catalytically active species from external degradation, and limiting trace metal contamination of the final products.[43,44] All heterogenized catalysts were fully characterized (see the SI, Section 14). Among them, nanocapsules loaded with palladium acetate, identified as Nc-Pd(OAc)$_2$, and those loaded simultaneously with palladium acetate and XPhos ligand (Nc-Pd(OAc)$_2$-XPhos) are of particular interest (details of their preparation are reported in Section 13 of the SI). Fig. 7 shows the SEM and HR-TEM images evidencing the spherical shape and regularity of the capsules, and energy dispersive spectroscopy (EDS)

Table 3 Optimization of reaction conditions for the Sonogashira coupling between 4-bromoanisole and phenylacetylene. Triethylamine (Et_3N) is used as the base. Borax-crosslinked Ncs are used as catalytic systems[a]

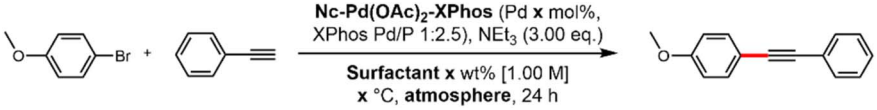

Entry	EC capsules (Pd mol%)	Surfactant (wt%)	T (°C)	Atmosphere	GC-MS conv. to product %
1	Nc-Pd(OAc)$_2$ (0.75) + free XPhos	K-EL (2)	rt	Air	—
2	Nc-Pd(OAc)$_2$ (0.75) + free XPhos	K-EL (5)	rt	Air	—
3	Nc-Pd(OAc)$_2$ (0.75) + free XPhos	K-EL/Tol 9 : 1 (2)	rt	Air	—
4	Nc-Pd(OAc)$_2$ (0.75) + free XPhos	—	rt	Air	—
5	Nc-Pd(OAc)$_2$-XPhos (0.75)	K-EL (2)	rt	Air	4
6	Nc-Pd(OAc)$_2$-XPhos (1.50)	K-EL (2)	rt	Air	4
7	Nc-Pd(OAc)$_2$-XPhos (2.00)	K-EL (2)	rt	Air	17
8	Nc-Pd(OAc)$_2$-XPhos (0.75)	K-EL (2)	45	Air	5
9	Nc-Pd(OAc)$_2$-XPhos (0.75)	K-EL (2)	rt	N_2	79, 30, 93, 52
10	Nc-Pd(OAc)$_2$-XPhos (0.75)	K-EL (2)	16	N_2	12
11	Nc-Pd(OAc)$_2$-XPhos (0.75)	K-EL (2)	35	N_2	47
12	**Nc-Pd(OAc)$_2$-XPhos (0.75)**	**K-EL (2)**	**45**	**N_2**	**100, 98, 100 (6 h)**
13	**Mc-Pd(OAc)$_2$-XPhos (0.75)**	**K-EL (2)**	**45**	**N_2**	**100**

[a] GC-MS conversion % are determined by the ratio of the integration of product and starting material peaks.

highlighting colocalization of Pd ad P atoms and thus the integrity of the catalyst. It was not possible to observe any specific localization of the catalytic species within the capsules.

Catalytic activity was assessed using the Sonogashira coupling between 4-bromoanisole and phenylacetylene in 2 wt% aqueous solution of the industrial surfactant Kolliphor EL (K-EL) and with palladium acetate and XPhos as the catalytic system, according to our previous experience.[45] Sonogashira coupling in aqueous media is of particular interest in the growing field of green manufacturing of organic semiconductors.[43,46] Initial experiments using Nc-Pd(OAc)$_2$ with externally added XPhos showed negligible conversion under air, regardless of surfactant concentration or cosolvent addition (Table 3, entries 1–4).

Encapsulation of both Pd(OAc)$_2$ and XPhos improved the reactivity modestly (5–17% conversion; entries 5–7), which increased markedly under a nitrogen atmosphere (entry 9).

Raising the reaction temperature to 45 °C yielded quantitative conversions in multiple trials (entry 12), and significantly improved the reproducibility compared to reactions performed at room temperature.[47] The lack of reproducibility is a well-known limit of micellar catalysis, and it's often addressed through the addition of a small amount of an organic cosolvent.[48]

In the present system, the same effect could be achieved by a modest increase in temperature, suggesting that mass transport rather than intrinsic catalytic activity is the limiting factor under milder conditions. We therefore propose that diffusion of the reagents through the polymeric matrix and/or across the capsule–micelle interface represents the dominant barrier to effective catalyst engagement at room temperature. Increasing the temperature likely enhances capsule permeability and molecular diffusion, thereby facilitating access to the encapsulated catalytic sites.

Importantly, comparable catalytic activity was observed for both micro- and nanocapsules under optimized conditions (entry 13). This indicates that catalysis is not strictly governed by the external surface area of the capsules, and suggests that the active species are accessible to the reaction medium either through permeation of the shell or at dynamic interfaces between the capsules and the micellar environment. Taken together, these observations support a model in which catalytic turnover is enabled by temperature-assisted diffusion rather than by direct surface exposure of the catalyst. With the optimal conditions established, we subsequently explored the generality of the reaction (Scheme 2). The coupling proceeds smoothly on aryl (**1**, **5**, **6**) and heteroaryl (**2**, **3**, **4**, **7**) bromides, both electron rich and electron poor. Alkynes bearing both aliphatic and aromatic substituents are tested successfully. In general, the observed reactivity matches that of analogous reactions performed under the same conditions but with the homogeneous catalysts.[45] In particular, analogous (quantitative) conversions to products **1**, **2** and **7** were achieved working with either Nc-Pd(OAc)$_2$-XPhos or using directly Pd(OAc)$_2$ and XPhos in the same amount, with main differences in yields due to the different purification protocols adopted.

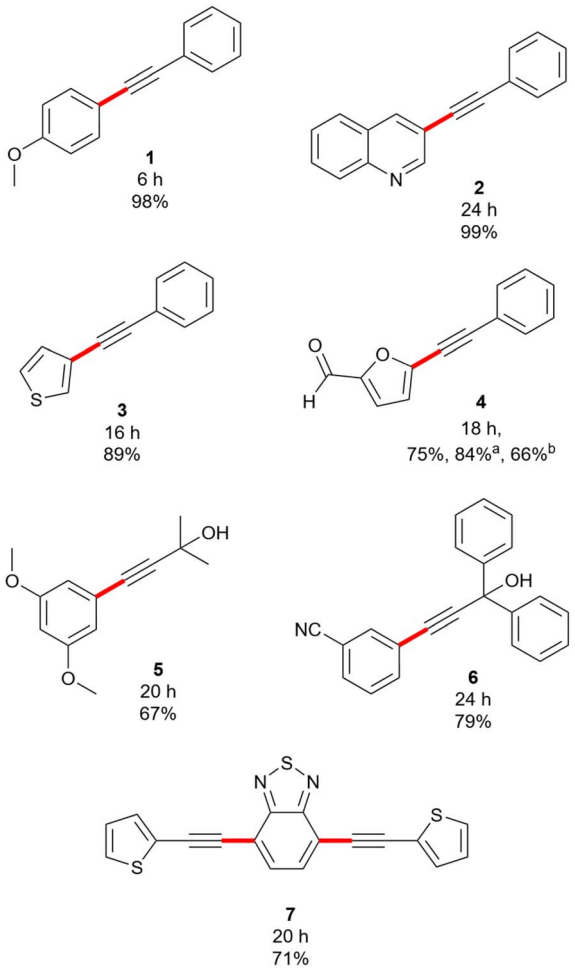

Scheme 2 Sonogashira coupling products obtained under optimized conditions (2 mmol scale). ArBr (1 eq.), alkyne (1 eq.), Nc-Pd(OAc)$_2$-XPhos (0.75 mol%), Et$_3$N (3 eq.), 2% K-EL in H$_2$O, 45 °C, N$_2$. [a]Reaction run on 4 mmol scale. [b]Reaction run using the catalyst recycled from the previous run.

While in terms of catalytic loading and yield the use of supported catalysts does not provide clear-cut benefits with respect to standard homogeneous phase catalysts, the purity of the product is dramatically impacted. Metal contamination is a severe issue in both pharmaceutical and materials chemistry.

While working under otherwise identical conditions, the residual Pd contamination in the coupling product was reduced by a factor of around 2.5 (evaluated by ICP-OES analysis, details in the SI, Section 19), whenever working with borax encapsulated catalysts. To confirm the capability of the Ncs to prevent the release of Pd in the solution, we also submitted the Nc-Pd(OAc)$_2$-XPhos capsules to a leaching test in a 2 wt% K-EL solution and Et$_3$N and – after filtration of the capsules – we used that medium to carry out the model Sonogashira reaction. Even after 24 hours, we observed no conversion (SI, Section 18).

Alongside the benefits in streamlining the purification, heterogeneous catalysis also enables recycling. We preliminarily tested the recovery and recycle of our Ncs, using the reaction of 2-bromo-5-formylfuran and phenylacetylene to give

derivative **4** as the testbed. Due to the small catalytic loading allowed by our procedure, we had to run this specific reaction on the 4 mmol scale to be able to work with a sample of nanocapsules large enough to ensure efficient recovery and reuse. As shown in Scheme 2, scaling up the reaction benefited its efficiency as the yield went from 75% to 84%. The yield drops to 66% in the second run, possibly because of partial oxidation of the catalyst as we did not perform the work up under a nitrogen atmosphere as it was impractical for the present study (all the details are in the SI, Section 20). We also considered the possibility to perform the Suzuki–Miyaura (S–M) reaction, known to be particularly performing under micellar catalysis and of perhaps greater generality for the synthesis of conjugated materials. While the reaction performed remarkably well, at catalyst loading as low as 400 ppm, we gathered evidence that boronic acids react with the TMPG-EC shell, opening the epoxides and possibly replacing the boric acid (SI, Section 16). While this process does not impair the S–M reaction as the EC supported boronic acid remains reactive in the coupling, the process leads to degradation of the capsules and leaching of the catalyst, thus dramatically reducing the competitive advantage of heterogeneous over homogeneous catalysis.

Conclusions

We have developed a cost-effective methodology that represents a significant advancement in the field of encapsulation, addressing sustainability concerns and enhancing the overall mass recovery efficiency, while focusing on scalability and versatility as well. Differently from the literature approach requiring isolation and crosslinking as distinct steps, we devised a one-step crosslinking strategy avoiding particle sintering and enabling nanoscale confinement without solid-state curing. The approach establishes a generalizable platform where crosslinking density and surface chemistry can be modularly tuned after capsule formation, at the same time offering sizeable advantages in terms of recovery. We have then explored the application of resulting capsules in catalysis, by assembling Pd-loaded nanoreactors which revealed remarkable catalytic activity in Sonogashira cross-coupling reactions carried out in water as the only solvent. Suzuki–Miyaura coupling can also be performed, although the capsule catalysts cannot be recovered intact at the end of the reaction. Our method offers dramatic improvements in the reduction of metal contamination in the coupling product and shows potentiality for recovery and reuse of the catalyst thus further highlighting its relevance as a green chemistry compliant approach.

Author contributions

Conceptualization: E. G., L. B. Investigation: E. G., S. Me., A. Fa., A. Fr., S. Ma. Data curation: E. G., S. Ma. Supervision: S. Ma., L. B. Writing – original draft: E. G., S. Me., A. Fa., A. Fr. Writing – review & editing: S. Ma., L. B. Funding acquisition: L. B.

Conflicts of interest

There are no conflicts to declare.

Data availability

The data supporting this article have been included as part of the supplementary information (SI). Supplementary information: materials and methods, general procedure for the synthesis of the nanocapsules, SEM images, crosslinking approaches, dynamic light scattering data, discussion of the green chemistry metrics, thermal and morphological characterization, Suzuki Miyaura couplings, leaching of the catalyst, NMR data. See DOI: https://doi.org/10.1039/d6na00071a.

Acknowledgements

This work was supported by MIUR under the 2017YXX8AZ PRIN and PRIN PNRR – P2022PXS5S_002 grant. L. B. acknowledges the MUSA – Multilayered Urban Sustainability Action – project (contract number ECS 000037), funded by the European Union – NextGenerationEU, under the National Recovery and Resilience Plan (NRRP) Mission 4 Component 2 Investment Line 1.5: Strengthening of research structures and creation of R&D "innovation ecosystems", set up by "territorial leaders in R&D".

References

1 V. Suganya and V. Anuradha, *Int. J. Pharm. Clin. Res.*, 2017, **9**, 233–239.
2 P. N. Ezhilarasi, P. Karthik, N. Chhanwal and C. Anandharamakrishnan, *Food Bioprocess Technol.*, 2013, **6**, 628–647.
3 B. Šumiga, B. Šumiga, D. Ravnjak and B. Boh Podgornik, *Coatings*, 2019, **9**, 470.
4 X.-C. Song, Y.-L. Yu, G.-Y. Yang, A.-L. Jiang, Y. Ruan and S. Fan, *Colloids Surf., B*, 2022, **216**, 112560.
5 K. Chen, C. Xu, J. Zhou, R. Zhao, Q. Gao and C. Wang, *Carbohydr. Polym.*, 2020, **232**, 115821.
6 N. Gorji, M. Jahanshahi, M. H. Shahavi and N. Ayrilmis, *Int. J. Biol. Macromol.*, 2025, **321**, 146336.
7 S. Kamel, N. Ali, K. Jahangir, S. M. Shah and A. A. El-Gendy, *Express Polym. Lett.*, 2008, **2**, 758–778.
8 Z. Li, D. Zhang, J. Weng, B. Chen and H. Liu, *Carbohydr. Polym.*, 2014, **99**, 748–754.
9 W. Qin, Z. Li, J. Li, L. Zhang, R. Liu and H. Liu, *Cellulose*, 2015, **22**, 203–214.
10 V. Marturano, H. Marcille, P. Cerruti, N. A. Bandeira, M. Giamberini, A. Trojanowska, B. Tylkowski, C. Carfagna, G. Ausanio and V. Ambrogi, *ACS Appl. Nano Mater.*, 2019, **2**, 4499–4506.
11 B. Iyisan and K. Landfester, *Macromol. Rapid Commun.*, 2019, **40**, 1800577.
12 K. A. Mahmoud, J. A. Mena, K. B. Male, S. Hrapovic, A. Kamen and J. H. T. Luong, *ACS Appl. Mater. Interfaces*, 2010, **2**, 2924–2932.
13 G. Murtaza, *Acta Pol. Pharm.*, 2012, **69**, 11–22.

14 P. Brazzo, *PhD thesis*, University of Milano-Bicocca, 2018.
15 C. Liu, Z. Rao, J. Zhao, Y. Huo and Y. Li, *Nano Energy*, 2015, **13**, 814–826.
16 N. Al Khouri Fallouh, L. Roblot-Treupel, H. Fessi, J. P. Devissaguet and F. Puisieux, *Int. J. Pharm.*, 1986, **28**, 125–132.
17 P. Ahmadi, A. Jahanban-Esfahlan, A. Ahmadi, M. Tabibiazar and M. Mohammadifar, *Food Rev. Int.*, 2022, **38**, 685–732.
18 S. K. Paswan and T. R. Saini, *Pharm. Res.*, 2017, **34**, 2779–2786.
19 S. Abbaspoor, A. Ashrafi and M. Salehi, *Colloid Polym. Sci.*, 2018, **296**, 1509–1514.
20 Z. Gul and K. Iqbal, *J. Nat. Fibers*, 2022, **19**, 14422–14434.
21 Y. Tian, Y. Cao, Y. Wang, W. Yang and J. Feng, *Adv. Mater.*, 2013, **25**, 2980–2983.
22 T. Harifi and M. Montazer, *Carbohydr. Polym.*, 2012, **88**, 1125–1140.
23 P. Tingaut, R. Hauert and T. Zimmermann, *J. Mater. Chem.*, 2011, **21**, 16066.
24 Y. Kim, D. Jeong, V. V. Shinde, Y. Hu, C. Kim and S. Jung, *Int. J. Biol. Macromol.*, 2020, **163**, 824–832.
25 J. Tang, J. Sisler, N. Grishkewich and K. C. Tam, *J. Colloid Interface Sci.*, 2017, **494**, 397–409.
26 Y. Lu and W. Yuan, *ACS Appl. Mater. Interfaces*, 2017, **9**, 29167–29176.
27 N. Aliasgharlou, F. Asghari Sana, S. Khoshbakht, P. Zolfaghari and H. Charkhian, *Turk. J. Chem.*, 2020, **44**, 1723–1732.
28 M. Hasani, E. D. Cranston, G. Westman and D. G. Gray, *Soft Matter*, 2008, **4**, 2238–2244.
29 E. Lam, K. B. Male, J. H. Chong, A. C. W. Leung and J. H. T. Luong, *Trends Biotechnol.*, 2012, **30**, 283–290.
30 H. Peng, C. Q. Yang and S. Wang, *Carbohydr. Polym.*, 2012, **87**, 491–499.
31 A. Pei, N. Butchosa, L. A. Berglund and Q. Zhou, *Soft Matter*, 2013, **9**, 2047.
32 D. Prasanthi, S. A. Rajguru, C. Aishwarya and A. Rahman, *J. Pharm. Res. Int.*, 2021, 649–663.
33 J. K. Pandey, W. S. Chu, C. S. Kim, C. S. Lee and S. H. Ahn, *Composites, Part B*, 2009, **40**, 676–680.
34 C. Q. Yang, D. Chen, J. Guan and Q. He, *Ind. Eng. Chem. Res.*, 2010, **49**, 8325–8332.
35 B.-H. Kim, J. Jang and S.-W. Ko, *Fibers Polym.*, 2000, **1**, 116–121.
36 P. De Cuadro, T. Belt, K. S. Kontturi, M. Reza, E. Kontturi, T. Vuorinen and M. Hughes, *React. Funct. Polym.*, 2015, **90**, 21–24.
37 T. Stepišnik Perdih, M. Zupanc and M. Dular, *Ultrason. Sonochem.*, 2019, **51**, 298–304.
38 A. Chávez-Martínez, R. A. Reyes-Villagrana, A. L. Rentería-Monterrubio, R. Sánchez-Vega, J. M. Tirado-Gallegos and N. A. Bolivar-Jacobo, *Foods*, 2020, **9**, 1688.
39 X. Geng, Y. Wang, N. Han, X. Zhang and W. Li, *Sol. Energy Mater. Sol. Cells*, 2021, **222**, 110938.
40 S. Tanpichai and K. Oksman, *J. Appl. Polym. Sci.*, 2018, **135**, 45710.
41 J. G. De Vries and S. D. Jackson, *Catal. Sci. Technol.*, 2012, **2**, 2009.
42 A. Zarour, S. Omar and R. Abu-Reziq, *Polymers*, 2021, **13**, 2566.
43 Z. Lu, J. B. Jasinski, S. Handa and G. B. Hammond, *Org. Biomol. Chem.*, 2018, **16**, 2748–2752.
44 B. H. Lipshutz and J. Matthey, *Technol. Rev.*, 2023, **67**, 278–284.
45 E. Ghiglietti, E. Incarbone, S. Mattiello and L. Beverina, *Eur. J. Org Chem.*, 2024, e202400223.
46 V. P. W. Böhm and W. A. Herrmann, *Eur. J. Org Chem.*, 2000, **2000**, 3679–3681.
47 C. Ceriani, E. Ghiglietti, M. Sassi, S. Mattiello and L. Beverina, *Org. Process Res. Dev.*, 2020, **24**, 2604–2610.
48 C. M. Gabriel, N. R. Lee, F. Bigorne, P. Klumphu, M. Parmentier, F. Gallou and B. H. Lipshutz, *Org. Lett.*, 2017, **19**, 194–197.